

Night-Side Relativistic Electron Precipitation Bursts in the Outer Radiation Belt: Insights from ELFIN and THEMIS

Xi Lu ¹, Xiao-Jia Zhang ¹, Anton V. Artemyev ², Vassilis Angelopoulos ²,
Jacob Bortnik ²

¹Department of Physics, University of Texas at Dallas, Richardson, Texas, USA

²University of California, Los Angeles, Los Angeles, California, USA

Key Points:

- We present a statistical study of unexpected relativistic electron precipitation bursts in the night-side outer radiation belt
- We show that these precipitating bursts are likely driven by whistler-mode waves that propagate to middle latitudes
- We parameterize the precipitating electron spectra for further applications in magnetosphere-ionosphere coupling models

arXiv:2411.19232v1 [physics.space-ph] 28 Nov 2024

Corresponding author: Xi Lu, xi.lu@utdallas.edu

Abstract

Electromagnetic whistler-mode waves play a crucial role in the acceleration and precipitation of radiation belt electrons. Statistical surveys of wave characteristics suggest that these waves should preferentially scatter and precipitate relativistic electrons on the day side. However, the night-side region is expected to be primarily associated with electron acceleration. The recent low-altitude observations reveal relativistic electron precipitation in the night-side region. In this paper, we present statistical surveys of night-side relativistic electron losses due to intense precipitation bursts. We demonstrate that such bursts are associated with storm time substorm injections and are likely related to relativistic electron scattering by ducted whistler-mode waves. We also speculate on the role of injections in creating conditions favorable for relativistic electron precipitation.

1 Introduction

Electron resonant scattering by electromagnetic whistler-mode waves, particularly by the most intense whistler-mode chorus waves, is the primary driver of energetic electron losses in the outer radiation belt (Bortnik & Thorne, 2007; Millan & Thorne, 2007; Li & Hudson, 2019). These wave-particle interactions result in electron pitch-angle scattering, leading to their precipitation into the Earth’s atmosphere where they may significantly alter ionospheric characteristics (Seppälä et al., 2015; Mironova et al., 2019; Verronen et al., 2021; Miyoshi et al., 2021; Lyons et al., 2021; Nishimura et al., 2021).

The energy range of precipitating electrons is determined by two key characteristics of whistler-mode waves: the wave normal angle (WNA) and their latitudinal extent. Although the most intense whistler-mode waves are field-aligned chorus waves (Li et al., 2011; Agapitov et al., 2013, 2018), these waves cannot resonate with relativistic electrons near the equatorial source region, where the energy of resonant electrons near the loss cone is limited to approximately 100–200 keV (e.g., Summers et al., 2007b, 2007a; Ni et al., 2011). Therefore, to contribute to relativistic electron losses, whistler-mode waves should either be very oblique (Lorentzen et al., 2001; Mourenas et al., 2014; Artemyev et al., 2016; Gan et al., 2023) or propagate to middle latitudes away from the equator along the field lines, where resonance energies can exceed 500 keV (see discussions in Miyoshi et al., 2020, 2021; L. Chen et al., 2022; Artemyev, Zhang, et al., 2024; Kang et al., 2024). Middle-latitude oblique waves, as well as field-aligned waves, are mainly observed in the day-side magnetosphere. In contrast, on the night side, whistler-mode waves are mostly confined around the equatorial region (Bortnik et al., 2007; Agapitov et al., 2013, 2018; Santolík et al., 2014). This day-night asymmetry in wave local time distribution, coupled with different ratios of plasma to cyclotron frequencies, indicates that day-side and night-side whistler-mode waves play different roles in radiation belt models: waves on the night-side are mostly implicated in the acceleration of electrons to relativistic energies, while those on the day-side contribute to both energetic and relativistic electron losses (Meredith et al., 2003; Horne et al., 2005; Mourenas et al., 2014; Ma et al., 2018; Agapitov et al., 2019). The recent low-altitude observations of electron precipitation suggest that night-side whistler-mode waves also contribute to relativistic electron losses (see details in Shumko et al., 2021; Tsai et al., 2023, 2024). These losses occur as intense bursts of precipitation, reaching the strong diffusion limit and typically occurring well equatorward from the curvature scattering region (see examples in Artemyev, Zhang, et al., 2024; Kang et al., 2024). The mechanism underlying night-side relativistic precipitation is likely associated with a specific population of whistler-mode waves that can be ducted around plasma density gradients (Hanzelka & Santolík, 2019; Ke et al., 2021; Hosseini et al., 2021; Harid et al., 2024). These ducted waves can propagate to middle latitudes with high intensity (L. Chen et al., 2021, 2022) and scatter relativistic electrons (Miyoshi et al., 2020; Kang et al., 2024). Although this relatively small population of ducted whistler-mode waves may not significantly impact average (statistical) wave models, they likely play

a critical role in dictating night-side losses of relativistic electrons (see discussions in Artemyev et al., 2021; Artemyev, Zhang, et al., 2024; Tsai et al., 2024).

Observations of individual relativistic electron precipitation events (Douma et al., 2017; Shumko et al., 2021; Artemyev, Zhang, et al., 2024; Kang et al., 2024) and their statistical contributions to electron losses (Tsai et al., 2023, 2024; H. Chen et al., 2023) highlight the necessity of including these losses in magnetosphere-ionosphere coupling models (see the discussion in Zou et al., 2024). The significance lies in the fact that these precipitating electrons can drastically modify ionospheric properties below 100km (e.g., Seppälä et al., 2015; Oyama et al., 2017; Yu et al., 2018; Stepanov et al., 2021; Verroenen et al., 2021). Therefore, it is crucial to investigate and parameterize the characteristics of this precipitation, including the energy spectra of precipitating electrons and their variability under different geomagnetic conditions.

In this work, we construct a dataset of relativistic precipitation bursts on the night side and investigate their statistical properties using high-resolution measurements from the ELFIN CubeSats (Angelopoulos et al., 2020). These measurements provide detailed energy and full pitch-angle distributions. The identified bursts are detected equatorward from the curvature scattering region (isotropy boundary; see details in Wilkins et al., 2023, and reference therein), that is, well within the outer radiation belt where electron precipitation is primarily driven by whistler-mode waves. We fit the electron precipitation spectra with analytical functions and present the fitting parameters as functions of geomagnetic conditions and spatial location. These detailed characterizations of night-side precipitation can be readily incorporated into magnetosphere-ionosphere coupling models, improving their ability to predict ionospheric responses.

2 Datasets

Two identical CubeSats from the Electron Losses and Fields Investigation (ELFIN) mission were launched on September 15, 2018 and ended on September 30, 2022 (Angelopoulos et al., 2020). Each satellite is equipped with energetic particle detectors for ions (EPD-I) and electrons (EPD-E). Electrons are measured within an energy range of 50 keV to approximately 6 MeV, with an energy resolution ($\Delta E/E$) of less than 40 % and a time resolution (T_{spin}) of about 2.85 s (Angelopoulos et al., 2023; Tsai & et al., 2024). The high pitch-angle resolution of the EPD-E ($\Delta\alpha \simeq 22.5^\circ$) allows it to resolve the trapped electrons (outside the local bounce loss cone) from precipitating electrons (within the local bounce loss cone) (see details X.-J. Zhang, Angelopoulos, et al., 2022; Angelopoulos et al., 2023). The ratio of the precipitating electron flux and the trapped electron flux (J_{prec}/J_{trap}) indicates the efficiency of equatorial electrons being scattered by waves (Li et al., 2013; Mourenas et al., 2021; X.-J. Zhang, Artemyev, et al., 2022; Shen et al., 2022; Capannolo et al., 2023) or (and) by magnetic field line curvature (Wilkins et al., 2023; Zou et al., 2024).

Following previous case studies of energetic electron precipitation associated with whistler-mode waves (Tsai et al., 2022; Gan et al., 2023), we examine individual bursts of electrons scattered by whistler-mode waves. The main criteria for distinguishing these bursts from those driven by electromagnetic ion cyclotron (EMIC) waves (Angelopoulos et al., 2023) and curvature scatterings (Wilkins et al., 2023) are as follows: [1] All events are observed equatorward from the electron isotropy boundary (IB) (see details in Wilkins et al., 2023; Artemyev et al., 2023; Sergeev et al., 2023), which is the inner edge of the curvature scattering region; [2] For all events, the ratio J_{prec}/J_{trap} peaks at 50keV and decreases with increasing energy (which differs from events associated with EMIC waves, see discussions in Grach et al., 2022; Bashir et al., 2024), [3] All events exhibit $J_{prec}/J_{trap} > 0.5$ at relativistic energies ($\sim 500\text{keV}$) (see examples in Artemyev, Zhang, et al., 2024). In total, 169 events of relativistic electron precipitation bursts were detected on the night side ($MLT \in [20, 5]$) from ELFIN observations in 2021 and 2022.

Several night-side relativistic electron precipitation events captured by ELFIN are accompanied by near-equatorial observations from Time History of Events and Macroscale Interactions during Substorms (THEMIS) (Angelopoulos, 2008). We use spin-resolution (FGS, ~ 3 s) magnetic field data in geocentric solar magnetospheric (GSM) coordinates measured by the fluxgate magnetometer (Auster et al., 2008). Additionally, we analyze the wave magnetic field spectra data from the FFF dataset during fast survey mode (1 s time resolution) (Cully et al., 2008), utilizing search-coil magnetometer measurements (Le Contel et al., 2008). Electron density data is provided by the electrostatic analyzer (ESA) in the reduced mode (~ 3 s time resolution) (McFadden et al., 2008).

Figures 1 and 2 show two examples of ELFIN orbits from our night-side relativistic electron precipitation dataset. Panels (a) and (b) show the dynamic spectrum of trapped flux (J_{trap}) and the ratio of precipitating flux and trapped flux (J_{prec}/J_{trap}). The plasma sheet region, characterized by isotropic fluxes ($J_{prec}/J_{trap} \sim 1$), is seen well in high magnetic latitudes. In the event shown in Figure 1, the plasma sheet at $MLAT > 63^\circ$ (fully isotropic flux region with the upper energy of electrons going down to higher latitudes; see discussion in Artemyev, Angelopoulos, et al., 2022), with its inner edge marked by an electron isotropy boundary (IBe). Here, the dispersed precipitation pattern exhibits energies of isotropic fluxes increasing towards lower latitudes (see discussions of formation of this pattern in Wilkins et al., 2023; Artemyev et al., 2023; Sergeev et al., 2023, and references therein). Equatorward of the IBe, ELFIN detects three bursts of intense precipitation with $J_{prec}/J_{trap} \sim 1$ at 50 keV and $J_{prec}/J_{trap} > 0.1$ at 500 keV (indicated by the horizontal dashed line in panel (b)). For each burst, the average spectra of trapped and precipitating electrons are shown in panels (c), (d), and (e). The fluxes are quite similar, indicating the achievement of the strong diffusion limits on electron precipitation (Kennel, 1969). The maximum energies where precipitating spectra are above the noise level ($\sim 100 \text{ cm}^{-2}\text{s}^{-1}\text{sr}^{-1}\text{MeV}^{-1}$) reach up to 2 MeV, which is comparable to the most energetic microburst precipitation (see Douma et al., 2017, 2019; Meyer-Reed et al., 2023). The precipitating spectra are fitted with the function $const \cdot (E/E_0)^a \cdot \exp(-E/E_0)$ to quantify this relativistic precipitation, which combines power-law and exponential shapes (see examples of this fitting for precipitating fluxes in X.-J. Zhang, Angelopoulos, et al., 2022). For the first event, the typical energies of the exponential decay of precipitating fluxes are $E_0 \sim 100\text{--}200$ keV, with a around zero (Figure 1(c)-(e)). This suggests that there is no energy range with a power-law precipitation spectrum, and the entire precipitating flux follows the exponential spectrum of trapped electrons. The energy, $E_0 \sim 100\text{--}200$ keV, indicates that relativistic precipitating fluxes (around 1–2 MeV) are approximately 10^{-4} times smaller than fluxes of 50–100 keV electrons, which are typically associated with whistler-mode wave driven precipitation (e.g., Li et al., 2013; Ni et al., 2014; Mourenas et al., 2021; Tsai et al., 2023). E_0 can be slightly larger for trapped electrons because scattering at relativistic energies becomes less effective (Summers et al., 2007b), and fluxes decay faster with increasing energy for precipitating electrons (compare the blue and black lines in panels (c)-(e)). Note that J_{prec} being larger than J_{trap} above 500 keV is likely attributable to flux variability within the spin period of ELFIN rather than a physical effect, indicative of time aliasing due to the limited temporal resolution during rapidly varying dynamics (see discussion in X.-J. Zhang, Angelopoulos, et al., 2022).

Figure 2 illustrates that whistler-mode driven precipitation overlap with those driven by EMIC waves (panels (a), (b)). Precipitation bursts related to whistler-mode waves show a decreasing J_{prec}/J_{trap} ratio from sub-relativistic electron precipitation (< 500 keV) to relativistic energies. However, these bursts overlap with $J_{prec}/J_{trap} \sim 1$ precipitation due to EMIC waves at energies > 1 MeV (see Bashir et al., 2024, for additional examples of precipitation driven by a combination of whistler-mode and EMIC waves). The plasma sheet region, where electron fluxes are often below 300 keV with isotropic $J_{prec}/J_{trap} \sim 1$, is located at latitudes $> 69^\circ$, while all precipitation bursts are observed equatorward of this region (note that there is no clear IB for this event, a situation ob-

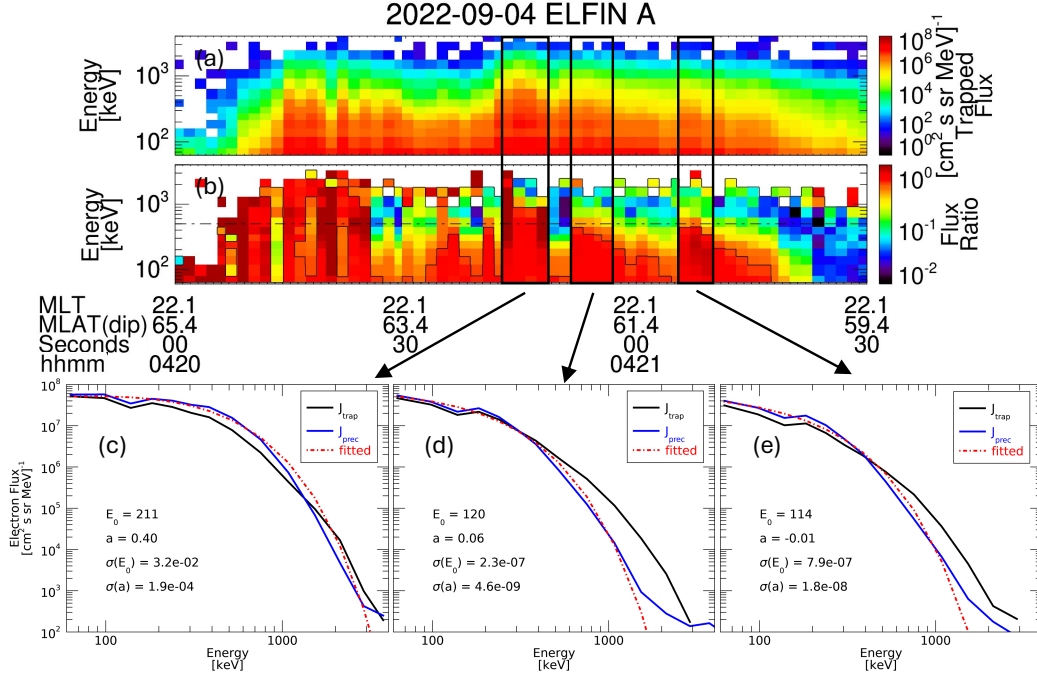


Figure 1. First example of night-side ELFIN observations of relativistic electron precipitation bursts from the outer radiation belt: (a) locally trapped electron fluxes, (b) precipitating-to-trapped flux ratio with precipitating bursts marked by black rectangles, (c)-(e) trapped and precipitating electron spectra within the relativistic bursts, with the precipitating spectrum fitted by $A \cdot (E/E_0)^a \cdot \exp(-E/E_0)$.

served in roughly 20% of night-side ELFIN orbits, see discussion in Wilkins et al., 2023; Artemyev, Sergeev, et al., 2024). The fitting procedure effectively excludes the EMIC-driven precipitation spectrum and covers only the core precipitation below 500 keV, which is driven by whistler-mode waves. Although we cannot fully distinguish precipitation drivers at intermediate energies (500 ~ 1000 keV), where EMIC waves might cause electron losses through non-resonant or nonlinear wave-particle interactions (see An et al., 2022, 2024; Grach & Demekhov, 2023; Hanzelka et al., 2023), the fitting does not include purely EMIC-dominated losses at > 1 MeV. The main difference between the precipitation bursts shown in Figures 1(c-e) and 2(c-f) is the a parameter of the fitting: in Figure 1, $a \geq 0$ (with a plateau around 100 – 200 keV), whereas in Figure 2, $a \leq 0$ (with rapid flux decreases as energy increases, even around 100–200 keV). Both sets of bursts show strong diffusion limits ($J_{prec}/J_{trap} \sim 1$ at < 500 keV) so the spectral differences ($a > 0$ versus $a < 0$) are attributed to variations in the trapped electrons.

Figures 1 and 2 have shown typical bursts of whistler-mode wave driven relativistic electron precipitation in the night-side inner magnetosphere (with average MLT values of 22 and 0.5 for these two ELFIN orbits). We compile statistics on such bursts and fit the precipitating spectra to investigate the dependencies of E_0 and a on geomagnetic activity. For each burst, we also determine E_{max} as an energy where the level of flux goes down to $J_{prec} = 100 \text{ cm}^{-2}\text{s}^{-1}\text{sr}^{-1}\text{MeV}^{-1}$, i.e., E_{max} represents the maximum energy of precipitating fluxes above the noise level.

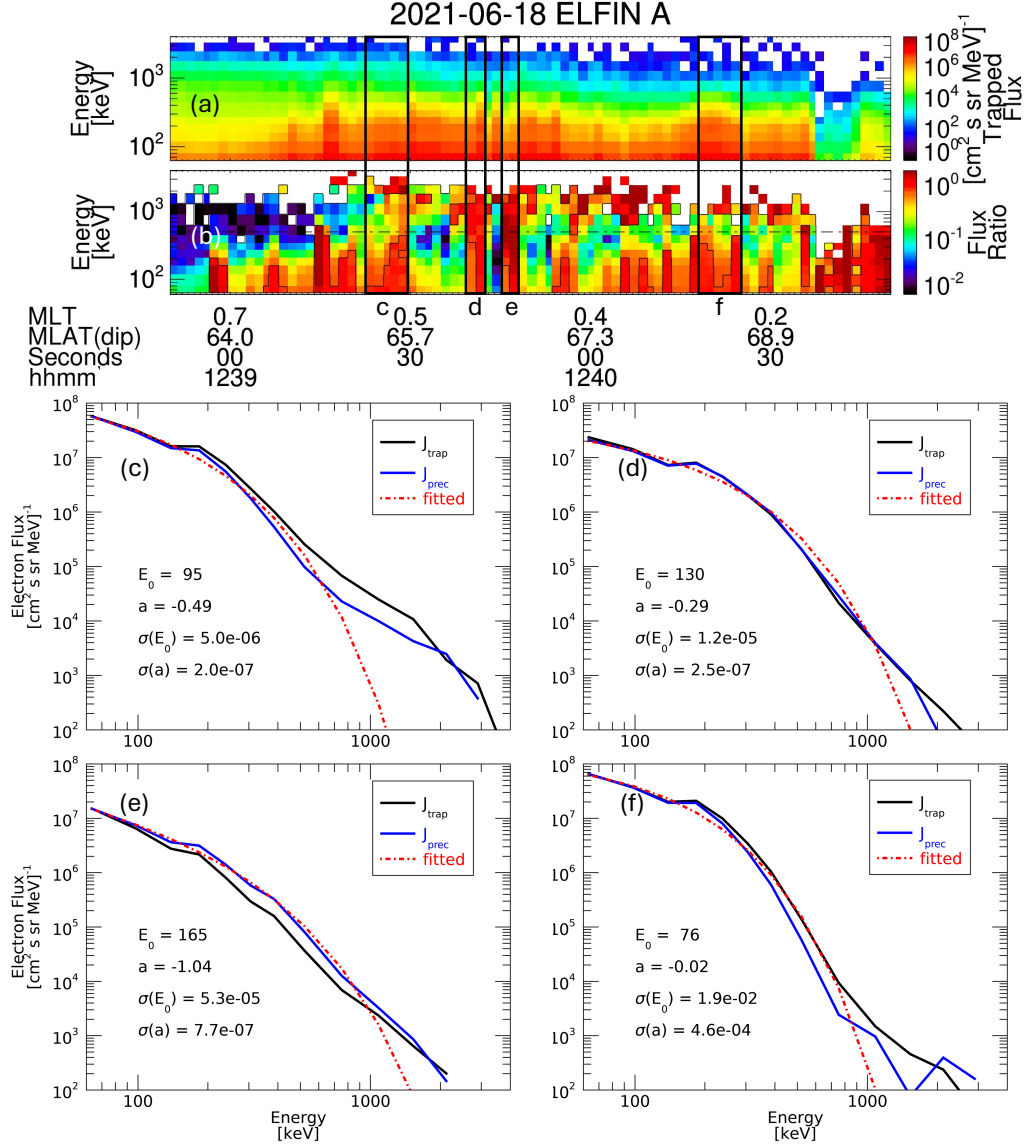


Figure 2. Second example of night-side ELFIN observations of relativistic electron precipitation bursts from the outer radiation belt: (a) locally trapped electron fluxes, (b) precipitating-to-trapped flux ratio with precipitating bursts marked by black rectangles, (c)-(f) trapped and precipitating electron spectra within the relativistic bursts, with the precipitating spectrum fitted by $A \cdot (E/E_0)^a \cdot \exp(-E/E_0)$.

3 Statistical properties of relativistic precipitation bursts

Figure 3 shows the statistical characteristics of 169 precipitation bursts with $E_{\max} > 500$ keV. Almost all events are observed within the $[60, 70^\circ]$ latitudinal range corresponded to the outer radiation belt in the night-side magnetosphere (panel (a)). The latitudinal range of these bursts is about $\Delta MLTA \leq 0.4^\circ$ (panel (b)), which corresponds to $\Delta r \leq 3000$ km when projected onto the equatorial plane (see details of projections in the night-side in Artemyev, Sergeev, et al., 2024). This spatial scale is typical for whistler-mode wave source regions associated with plasma sheet injections (Agapitov et al., 2017; X.-J. Zhang et al., 2023) as well as for whistler-mode chorus wave source regions in the outer radiation belt (e.g., Santolík & Gurnett, 2003; Agapitov et al., 2011). Interestingly, most relativistic electron bursts are observed either in the pre-midnight sector (panel (c)), where most injections occur (Gabrielse et al., 2014), or in the post-midnight sector, despite the latter being well known for whistler-mode wave activity (e.g., Agapitov et al., 2018). We suggest that relativistic electron precipitation requires not only wave activity, but also gradients in background plasma density and magnetic field associated with injections that can guide waves (see the Discussion section and (Artemyev, Zhang, et al., 2024; Kang et al., 2024)). Without such gradients, the waves generated by dawnward-drifting electrons (Tao et al., 2011) would be confined around the equator (Meredith et al., 2012) and scatter only sub-relativistic electrons. The importance of injections for relativistic electron precipitation is further supported by panels (i) and (j), which show that relativistic precipitation events are associated with strong geomagnetic activity. Most events occur with SME (an analog of the AE index) above 300 nT (Gjerloev, 2012) during the substorm expansion/recovery phase associated with plasma sheet injections. Additionally, the majority of events happen during storms, meaning they are storm-time injections, with the SYM-H index smaller than -30 nT (see discussion about the efficiency of storm-time injections and energetic particle transport in Beyene et al., 2022; Beyene & Angelopoulos, 2024). Specifically, 146 out of 169 (86%) events are associated with storms where the SYM-H minimum is below -50 nT, with 51% observed during the storm main phase and 49% during the recovery phase.

Typical energies from the fitting of electron precipitation spectra, E_0 , are usually < 200 keV (panel (e)), while the parameter a is around zero or negative (panel (d)). This indicates that the precipitating electron fluxes decrease rapidly with increasing energy, with the flux ratio at 50 keV being approximately 10^4 larger than at $\sim 1-2$ MeV. The small absolute value of a suggests that the precipitating spectra follow an exponential distribution. The average magnitude of the precipitating flux at 50 keV is $A \approx 4.5 \times 10^7 \text{ cm}^{-2}\text{s}^{-1}\text{sr}^{-1}\text{MeV}^{-1}$. Thus, the statistics from panels (d) and (e) can be used to define the range of relativistic night-side electron precipitation using the fitting function $A \cdot (E/E_0)^a \cdot \exp(1/2 - E/E_0)$. Panel (f) shows the maximum energy of the precipitating electrons is about a factor of 10 – 20 of E_0 for most events. Therefore, this fitting function should be applicable for energies $E < 2$ MeV, assuming a typical $E_0 \sim 100$ keV.

Using the resonance condition for field-aligned whistler-mode waves and the cold plasma dispersion relation (Lyons & Williams, 1984), we evaluate the magnetic latitudes at which electron scattering occurs at E_{\max} for our dataset of relativistic bursts (see similar calculations in Roosnov et al., 2024; Artemyev, Zhang, et al., 2024). One key parameter in determining the resonance latitude is the ratio of the plasma frequency to the electron cyclotron frequency, $\Omega_{pe,eq}/\Omega_{ce,eq}$, which depends on the plasma density. We consider two scenarios: (1) $\Omega_{pe,eq}/\Omega_{ce,eq} \approx L$ from the model by Sheeley et al. (2001) (Sheeley et al., 2001) and (2) $\Omega_{pe,eq}/\Omega_{ce,eq} = 2$, which aligns with observations of significant plasma density reduction during geomagnetically active periods, such as substorm injections (Agapitov et al., 2019). The distribution of plasma density along magnetic field lines is based on the model by (Denton et al., 2006). Panels (g) and (h) show the results of the resonance latitudes evaluated at the loss-cone pitch angle for precipitating elec-

trons and E_{\max} . For both $\Omega_{pe,eq}/\Omega_{ce,eq}$ approximations, most events show scattering latitudes above 30° , which is significantly higher than the maximum latitudes of night-side whistler-mode waves (Meredith et al., 2012; Agapitov et al., 2013). Therefore, these relativistic precipitation bursts suggest the presence of a small population of ducted waves capable of propagating to middle latitudes ($\geq 30^\circ$) and scattering electrons there.

Figure 4 (a) shows the average spectrum of the precipitating-to-trapped electron flux ratio for the entire dataset of events. Data points with $J_{prec}/J_{trap} > 1.2$ were excluded because such measurements are associated with limitations of ELFIN measurements (see X.-J. Zhang, Angelopoulos, et al. (2022)). The average flux ratio is close to the strong diffusion limit at 50 keV ($\langle J_{prec}/J_{trap} \rangle \sim 1$) and remains relatively high up to 1 MeV ($\langle J_{prec}/J_{trap} \rangle \sim 0.3$). This supports our initial hypothesis that night-side relativistic precipitation bursts are associated with extremely high wave activity and are likely driven by plasma sheet injections.

Figures 4 (b) and 4 (c) show the dependence of the fitting parameters E_0 and a on geomagnetic activity. For weaker substorms, with $SME < 300$ nT, the precipitation bursts exhibit $E_0 > 150$ keV and $a < -1$, indicative of precipitation with a power-law spectrum in the [50, 300] keV range (see similar observations for microburst precipitation in Johnson et al., 2021; Shumko et al., 2023), along with exponential decay above these energies. In contrast, the vast majority of precipitation bursts observed across all SME values in the [300, 1500] nT range are characterized by purely exponential spectra, with $E_0 \leq 100$ keV and $a \sim 0$. This suggests that stronger geomagnetic activity does not preferentially increase relativistic electron precipitation but instead maintains E_0 at ~ 100 keV and proportionately increases all energies accordingly while retaining the exponential term of the precipitation spectrum about 10^{-4} times smaller at $\sim 1-2$ MeV compared to 50 – 100 keV.

4 Discussion and concluding remarks

In this study, we investigated relativistic electron bursts observed by the low-altitude (low-Earth orbit) ELFIN CubeSats in the night-side inner magnetosphere. All burst occur equatorward of the inner edge of the electron plasma sheet and are very likely associated with electron scattering by whistler-mode waves. The precipitating-to-trapped flux ratio at 50 keV, with $\langle J_{prec}/J_{trap} \rangle \sim 1$, indicates that these bursts can be generated by intense waves (above 50pT; see Tsai et al., 2022). The high ratio at 1 MeV suggests that these waves are likely ducted, propagating from the equatorial source region to magnetic latitudes greater than 35° without significant damping (L. Chen et al., 2022; Kang et al., 2024). We attribute the generation of very intense whistler-mode waves and their ducting to the same phenomena associated with plasma sheet injections. (see also discussion in Artemyev, Zhang, et al., 2024). These injections can transport anisotropic electron populations (e.g., X. Zhang et al., 2018; Ukhorskiy et al., 2022) and lead to the generation of the most intense whistler-mode waves (e.g., Le Contel et al., 2009; Deng et al., 2010; Tao et al., 2011; X. Fu et al., 2014; Grigorenko et al., 2020). Additionally, plasma density gradients at injection fronts (dipolarization fronts) (Runov et al., 2011; Hwang et al., 2011) may contribute to wave ducting. To support this hypothesis, we examine two events from our statistics (two ELFIN orbits) for which THEMIS provides near-equatorial measurements in the same MLT sector as the ELFIN observations of relativistic electron precipitation. Figures 5 and 6 show coincident THEMIS observations during the ELFIN events in Figures 1 and 2.

The comparison between THEMIS and ELFIN is most representative of the event shown in Figures 1 and 5. THEMIS A, located at $MLT \sim 21$ and $L \sim 7$, observes a plasma sheet injection at 04:20 UT. A clear magnetic field dipolarization, characterized by an increase in B_z (panel (a)), occurs at the injection front (dipolarization front) (Nakamura et al., 2004; Runov et al., 2009). This front is associated with a strong plasma density

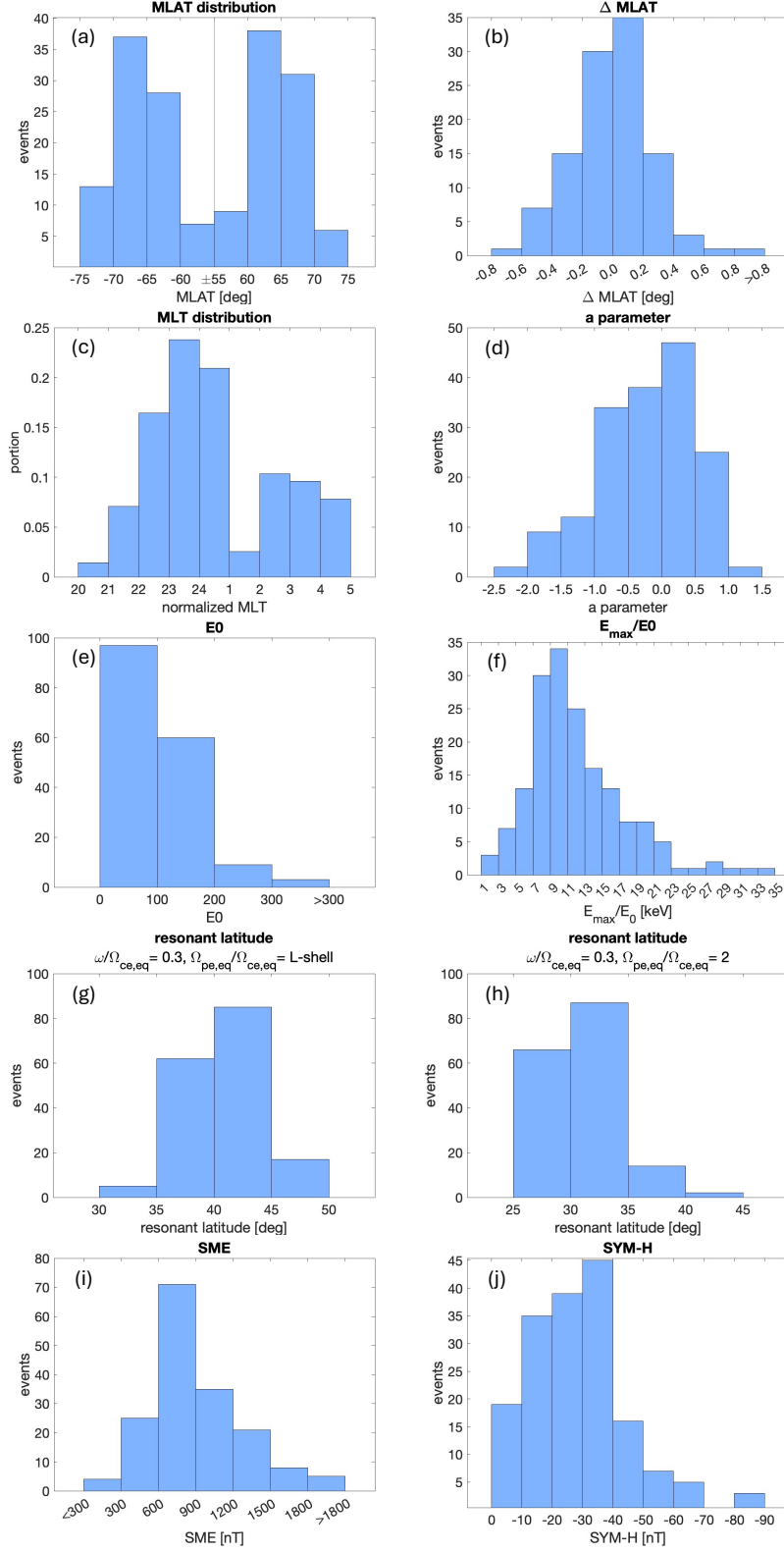


Figure 3. Histograms with distributions of (a)-(b) $MLAT$ and $\Delta MLAT$, (c) MLT , (d)-(f) a , E_0 and E_{max}/E_0 , (g)-(h) $MLAT_{res}$ for Ω_{pe}/Ω_{ce} from the (Sheeley et al., 2001) model and for $\Omega_{pe}/\Omega_{ce}=2$, (i) SME , and (j) $SYM-H$. In panel (c), the distribution is normalized by the total number of ELFV orbits within each MLT bin (see Tsai & et al., 2024).

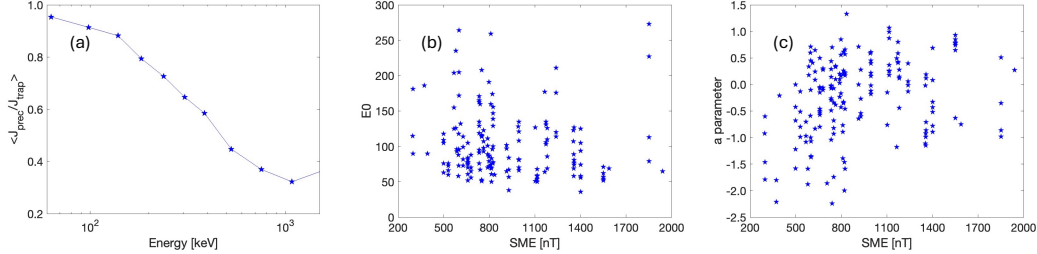


Figure 4. Average spectrum of the precipitating-to-trapped electron flux ratio (a). Scatter plots showing the distributions of events in the (SME, E_0) space (b), and in the (SME, a) space (c).

gradient (panel (b)) and a decrease in the ratio of the plasma frequency to the gyro frequency. After the front (from 04:20 to 04:30 UT), THEMIS A observes multiple plasma density fluctuations and structured whistler-mode wave emissions (panel (c)). Whistler-mode waves are likely generated by hot anisotropic electrons, which are consistently observed around the dipolarization front (e.g., H. S. Fu et al., 2013; Runov et al., 2013; X. Zhang et al., 2019; Breuillard et al., 2016). The density fluctuations and the strong gradient at the front can facilitate the trapping and ducting of these waves (see discussions in Hanzelka & Santolík, 2019; Streltsov & Bengtson, 2020; Streltsov & Goyal, 2021). Around the same time (04:20 UT), ELFIN A captures a series of relativistic precipitation bursts at $MLT \sim 22$, one hour from THEMIS A (see Figure 1). ELFIN’s observations are equatorward of the IBe, meaning these precipitation bursts may be projected closer to Earth than the injection observed by THEMIS (see statistics on the IBe location in Wilkins et al., 2023). Therefore, a plausible scenario involves an injection propagating earthward, with whistler-mode wave sources and density fluctuations facilitating wave ducting to the region of ELFIN observations (see one such example in Artemyev, Neishtadt, & Angelopoulos, 2022).

Figures 2 and 6 illustrate similar ELFIN/THEMIS observations of relativistic electron precipitation bursts around 12:40 UT at $MLT \sim 0.5$ and a plasma sheet injection at $MLT \sim 1$. THEMIS A, located below the equatorial plane, shows $B_x \sim -25$ nT and $B_z \sim 15$ nT (panel (a)), and thus may be projected further down the tail along magnetic field lines from its location at approximately $12R_E$. Similar to the event in Figures 1 and 5: THEMIS A observes an injection before it reaches the inner magnetosphere, which brings in whistler-mode wave sources associated with the relativistic electron precipitation observed by ELFIN. A strong plasma density gradient at the injection front (detected as a decrease in $|B_x|$ and an increase in B_z ; see details in (Nakamura et al., 2004; Runov et al., 2009)) and density fluctuations around the front are observed (panels (a) and (b)). Moreover, slightly ahead of the front, THEMIS A detects whistler-mode waves (panel (c)), characterized by peaks of wave activity around half of the electron gyrofrequency. These waves differ from the broad-band low-frequency turbulence, which is likely associated with kinetic Alfvén waves (Chaston et al., 2012; Malaspina et al., 2018). Therefore, the near-equatorial observations of THEMIS A (Figures 5 and 6) support our hypothesis that plasma sheet injections likely drive relativistic electron precipitation in the night-side magnetosphere. These injections transport whistler-mode sources and density gradients responsible for wave ducting to middle latitudes.

In conclusion, this study investigates relativistic electron precipitation on the night side through a statistical analysis of ELFIN observations. We show that:

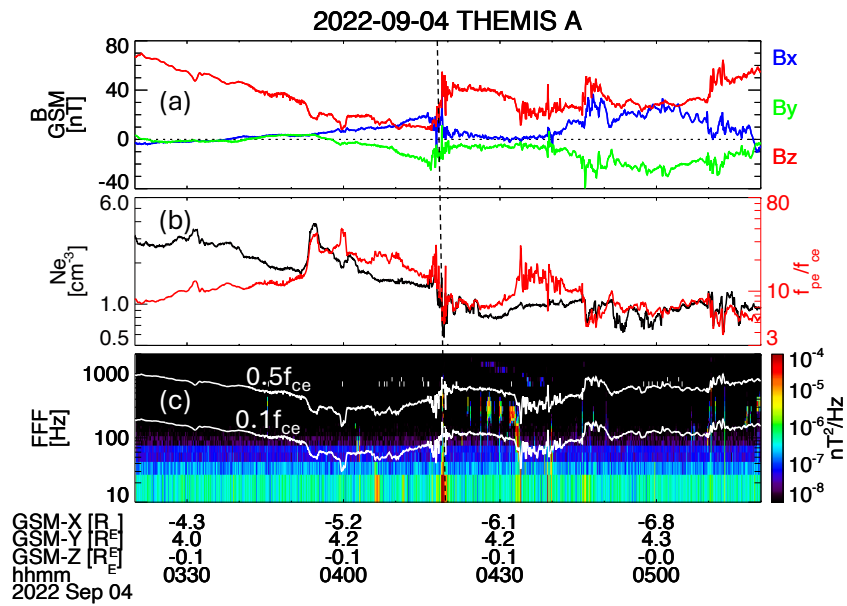


Figure 5. THEMIS A observations of the plasma injection conjugate to the ELFIN event from Figure 1: (a) magnetic field components in the GSM coordinates, (b) plasma density and the ratio of plasma frequency to electron gyrofrequency (f_{pe}/f_{ce}), and (c) the wave magnetic field spectra, with $f_{ce}/2$ and $f_{ce}/10$ shown by white lines. The vertical dashed line shows the approximate time of ELFIN’s observations of relativistic precipitation bursts, which is close to the injection time at THEMIS A.

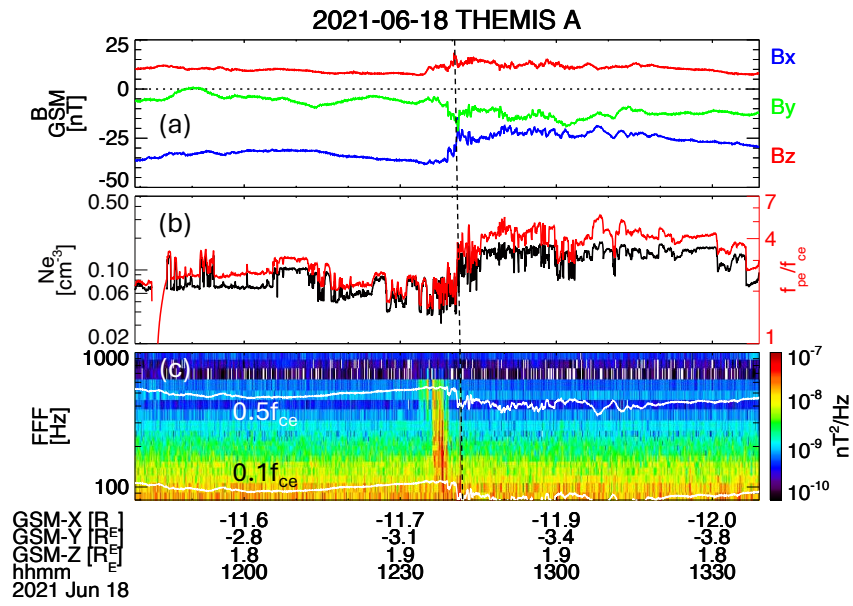


Figure 6. THEMIS A observations of the plasma injection conjugate to the ELFIN event from Figure 2: (a) magnetic field components in the GSM coordinates, (b) plasma density and the ratio of plasma frequency to electron gyrofrequency (f_{pe}/f_{ce}), and the(c) wave magnetic field spectra, with $f_{ce}/2$ and $f_{ce}/10$ shown by white lines. The vertical dashed line shows the approximate time of ELFIN’s observations of relativistic precipitation bursts, which is close to the injection time at THEMIS A.

- These precipitation bursts are linked to intense near-equatorial whistler-mode waves, which account for $J_{prec}/J_{trap} \sim 1$ at 50 keV and $J_{prec}/J_{trap} \sim 0.3$ at 1 MeV as they propagate to middle latitudes (with the resonance latitude $\sim 35^\circ$).
- The precipitating spectrum in the energy range of $< 1-2$ MeV can be approximated by $A \cdot (E/E_0)^a \cdot \exp(1/2 - E/E_0)$, with $A \approx 4.5 \times 10^7 \text{cm}^{-2} \text{s}^{-1} \text{sr}^{-1} \text{MeV}^{-1}$, $E_0 \approx 100$ keV, and $a \in [-0.5, 0.5]$.
- These precipitation bursts are associated with substorm activity ($SME > 300$ nT) and are likely driven by plasma sheet injections during the substorm expansion phase.
- The spatial extent of relativistic precipitation at $MLT \in [22, 1]$ and $MLAT \in [60^\circ, 70^\circ]$ is consistent with the idea that these bursts are related to substorm injections and are distinct from typical whistler-driven precipitation observed in the post-midnight sector.

These results suggest that relativistic precipitation bursts should be treated as a distinct precipitation band, which may have been overlooked in global models of radiation belt dynamics. Current models may not fully capture this phenomenon, which are often based on average whistler-mode wave statistics with strong wave intensity constraints around the equator (Meredith et al., 2012; Agapitov et al., 2013). The primary driver of these precipitation events is likely ducted whistler-mode waves, a wave population that has been under-investigated (see discussion in Artemyev, Zhang, et al., 2024; Kang et al., 2024). These night-side relativistic electron losses are significant for understanding radiation belt dynamics and may impact magnetosphere-ionosphere coupling at subauroral latitudes. These precipitation events could disturb the ionosphere below 100 km, influencing various ionospheric processes (see discussions in Oyama et al., 2017; Nishimura et al., 2021; Yu et al., 2022; Zou et al., 2024).

Acknowledgments

X.J.Z., A.V.A., and X.L. acknowledge support by NASA awards 80NSSC23K0108, 80NSSC23K1038, 80NSSC23K0100, 80NSSC24K0561, 80NSSC24K0138, 80NSSC19K0844, and NSF grant 2329897.

We are grateful to NASA's CubeSat Launch Initiative for ELFIN's successful launch in the desired orbits. We acknowledge early support of ELFIN project by the AFOSR, under its University Nanosat Program, UNP-8 project, contract FA9453-12-D-0285, and by the California Space Grant program. We acknowledge critical contributions of numerous volunteer ELFIN team student members. We acknowledge NASA contract NAS5-02099 for the use of data from the THEMIS Mission.

Open Research

Data was retrieved and analyzed using PySPEDAS and SPEDAS, see Angelopoulos et al. (2019).

References

- Agapitov, O. V., Artemyev, A., Krasnoselskikh, V., Khotyaintsev, Y. V., Mourenas, D., Breuillard, H., ... Rolland, G. (2013, June). Statistics of whistler mode waves in the outer radiation belt: Cluster STAFF-SA measurements. *J. Geophys. Res.*, *118*, 3407-3420. doi: 10.1002/jgra.50312
- Agapitov, O. V., Blum, L. W., Mozer, F. S., Bonnell, J. W., & Wygant, J. (2017, March). Chorus whistler wave source scales as determined from multipoint Van Allen Probe measurements. *Geophys. Res. Lett.*, *44*, 2634-2642. doi: 10.1002/2017GL072701

- Agapitov, O. V., Krasnoselskikh, V., Dudok de Wit, T., Khotyaintsev, Y., Pickett, J. S., Santolík, O., & Rolland, G. (2011, September). Multispacecraft observations of chorus emissions as a tool for the plasma density fluctuations' remote sensing. *J. Geophys. Res.*, *116*, 9222. doi: 10.1029/2011JA016540
- Agapitov, O. V., Mourenas, D., Artemyev, A., Hospodarsky, G., & Bonnell, J. W. (2019, June). Time Scales for Electron Quasi-linear Diffusion by Lower-Band Chorus Waves: The Effects of ω_{pe}/Ω_{ce} Dependence on Geomagnetic Activity. *Geophys. Res. Lett.*, *46*(12), 6178-6187. doi: 10.1029/2019GL083446
- Agapitov, O. V., Mourenas, D., Artemyev, A. V., Mozer, F. S., Hospodarsky, G., Bonnell, J., & Krasnoselskikh, V. (2018, January). Synthetic Empirical Chorus Wave Model From Combined Van Allen Probes and Cluster Statistics. *Journal of Geophysical Research (Space Physics)*, *123*(1), 297-314. doi: 10.1002/2017JA024843
- An, X., Artemyev, A., Angelopoulos, V., Zhang, X., Mourenas, D., & Bortnik, J. (2022, September). Nonresonant Scattering of Relativistic Electrons by Electromagnetic Ion Cyclotron Waves in Earth's Radiation Belts. *Phys. Rev. Lett.*, *129*(13), 135101. doi: 10.1103/PhysRevLett.129.135101
- An, X., Artemyev, A., Angelopoulos, V., Zhang, X.-J., Mourenas, D., Bortnik, J., & Shi, X. (2024, March). Nonresonant Scattering of Energetic Electrons by Electromagnetic Ion Cyclotron Waves: Spacecraft Observations and Theoretical Framework. *Journal of Geophysical Research (Space Physics)*, *129*(3), e2023JA031863. doi: 10.1029/2023JA031863
- Angelopoulos, V. (2008, December). The THEMIS Mission. *Space Sci. Rev.*, *141*, 5-34. doi: 10.1007/s11214-008-9336-1
- Angelopoulos, V., Cruce, P., Drozdov, A., Grimes, E. W., Hatzigeorgiu, N., King, D. A., ... Schroeder, P. (2019, January). The Space Physics Environment Data Analysis System (SPEDAS). *Space Sci. Rev.*, *215*, 9. doi: 10.1007/s11214-018-0576-4
- Angelopoulos, V., Tsai, E., Bingley, L., Shaffer, C., Turner, D. L., Runov, A., ... Zhang, G. Y. (2020, July). The ELFIN Mission. *Space Sci. Rev.*, *216*(5), 103. doi: 10.1007/s11214-020-00721-7
- Angelopoulos, V., Zhang, X. J., Artemyev, A. V., Mourenas, D., Tsai, E., Wilkins, C., ... Zarifian, A. (2023, August). Energetic Electron Precipitation Driven by Electromagnetic Ion Cyclotron Waves from ELFIN's Low Altitude Perspective. *Space Sci. Rev.*, *219*(5), 37. doi: 10.1007/s11214-023-00984-w
- Artemyev, A. V., Agapitov, O., Mourenas, D., Krasnoselskikh, V., Shastun, V., & Mozer, F. (2016, April). Oblique Whistler-Mode Waves in the Earth's Inner Magnetosphere: Energy Distribution, Origins, and Role in Radiation Belt Dynamics. *Space Sci. Rev.*, *200*(1-4), 261-355. doi: 10.1007/s11214-016-0252-5
- Artemyev, A. V., Angelopoulos, V., Zhang, X. J., Chen, L., & Runov, A. (2023, December). Dispersed Relativistic Electron Precipitation Patterns Between the Ion and Electron Isotropy Boundaries. *Journal of Geophysical Research (Space Physics)*, *128*(12), e2023JA032200. doi: 10.1029/2023JA032200
- Artemyev, A. V., Angelopoulos, V., Zhang, X. J., Runov, A., Petrukovich, A., Nakamura, R., ... Wilkins, C. (2022, October). Thinning of the Magnetotail Current Sheet Inferred From Low-Altitude Observations of Energetic Electrons. *Journal of Geophysical Research (Space Physics)*, *127*(10), e2022JA030705. doi: 10.1029/2022JA030705
- Artemyev, A. V., Demekhov, A. G., Zhang, X. J., Angelopoulos, V., Mourenas, D., Fedorenko, Y. V., ... Shinohara, I. (2021, November). Role of Ducting in Relativistic Electron Loss by Whistler-Mode Wave Scattering. *Journal of Geophysical Research (Space Physics)*, *126*(11), e29851. doi: 10.1029/2021JA029851
- Artemyev, A. V., Neishtadt, A. I., & Angelopoulos, V. (2022, April). On the Role of Whistler-Mode Waves in Electron Interaction With Dipolarizing Flux Bun-

- dles. *Journal of Geophysical Research (Space Physics)*, 127(4), e30265. doi: 10.1029/2022JA030265
- Artemyev, A. V., Sergeev, V. A., Angelopoulos, V., Zhang, X.-J., & Wilkins, C. (2024). Categorization of electron isotropy boundary patterns: ELFIN and POES observations. *ESS Open Archive*. doi: 10.22541/essoar.172526822.29644899/v1
- Artemyev, A. V., Zhang, X. J., Demekhov, A. G., Meng, X., Angelopoulos, V., & Fedorenko, Y. V. (2024, February). Relativistic Electron Precipitation Driven by Mesoscale Transients, Inferred From Ground and Multi-Spacecraft Platforms. *Journal of Geophysical Research (Space Physics)*, 129(2), e2023JA032287. doi: 10.1029/2023JA032287
- Auster, H. U., Glassmeier, K. H., Magnes, W., Aydogar, O., Baumjohann, W., Constantinescu, D., ... Wiedemann, M. (2008, December). The THEMIS Fluxgate Magnetometer. *Space Sci. Rev.*, 141, 235-264. doi: 10.1007/s11214-008-9365-9
- Bashir, M. F., Artemyev, A., Zhang, X.-J., Angelopoulos, V., Tsai, E., & Wilkins, C. (2024, May). Observations of Relativistic Electron Precipitation Due To Combined Scattering of Whistler-Mode and EMIC Waves. *Journal of Geophysical Research (Space Physics)*, 129(5), e2024JA032432. doi: 10.1029/2024JA032432
- Beyene, F., & Angelopoulos, V. (2024, May). Storm-Time Very-Near-Earth Magnetotail Reconnection: A Statistical Perspective. *Journal of Geophysical Research (Space Physics)*, 129(5), e2024JA032434. doi: 10.1029/2024JA032434
- Beyene, F., Angelopoulos, V., Runov, A., & Artemyev, A. (2022, June). Properties of Storm-Time Magnetic Flux Transport. *Journal of Geophysical Research (Space Physics)*, 127(6), e30357. doi: 10.1029/2022JA030357
- Bortnik, J., & Thorne, R. M. (2007, March). The dual role of ELF/VLF chorus waves in the acceleration and precipitation of radiation belt electrons. *Journal of Atmospheric and Solar-Terrestrial Physics*, 69, 378-386. doi: 10.1016/j.jastp.2006.05.030
- Bortnik, J., Thorne, R. M., & Meredith, N. P. (2007, August). Modeling the propagation characteristics of chorus using CRRES suprathermal electron fluxes. *Journal of Geophysical Research (Space Physics)*, 112(A8), A08204. doi: 10.1029/2006JA012237
- Breuillard, H., Le Contel, O., Retino, A., Chasapis, A., Chust, T., Mirioni, L., ... Nakamura, R. (2016, July). Multispacecraft analysis of dipolarization fronts and associated whistler wave emissions using MMS data. *Geophys. Res. Lett.*, 43, 7279-7286. doi: 10.1002/2016GL069188
- Capannolo, L., Li, W., Ma, Q., Qin, M., Shen, X. C., Angelopoulos, V., ... Hanzelka, M. (2023, November). Electron Precipitation Observed by ELFIN Using Proton Precipitation as a Proxy for Electromagnetic Ion Cyclotron (EMIC) Waves. *Geophys. Res. Lett.*, 50(21), e2023GL103519. doi: 10.1029/2023GL103519
- Chaston, C. C., Bonnell, J. W., Clausen, L., & Angelopoulos, V. (2012, September). Energy transport by kinetic-scale electromagnetic waves in fast plasma sheet flows. *J. Geophys. Res.*, 117, 9202. doi: 10.1029/2012JA017863
- Chen, H., Gao, X., Lu, Q., & Tsurutani, B. T. (2023, November). Global Distribution of Relativistic Electron Precipitation and the Dependences on Substorm Injection and Solar Wind Ram Pressure: Long-Term POES Observations. *Journal of Geophysical Research (Space Physics)*, 128(11), e2023JA031566. doi: 10.1029/2023JA031566
- Chen, L., Zhang, X.-J., Artemyev, A., Angelopoulos, V., Tsai, E., Wilkins, C., & Horne, R. B. (2022, March). Ducted Chorus Waves Cause Sub-Relativistic and Relativistic Electron Microbursts. *Geophys. Res. Lett.*, 49(5), e97559. doi: 10.1029/2021GL097559

- Chen, L., Zhang, X.-J., Artemyev, A., Zheng, L., Xia, Z., Breneman, A. W., & Horne, R. B. (2021, October). Electron microbursts induced by nonducted chorus waves. *Frontiers in Astronomy and Space Sciences*, *8*, 163. doi: 10.3389/fspas.2021.745927
- Cully, C. M., Ergun, R. E., Stevens, K., Nammari, A., & Westfall, J. (2008, December). The THEMIS Digital Fields Board. *Space Sci. Rev.*, *141*, 343-355. doi: 10.1007/s11214-008-9417-1
- Deng, X., Ashour-Abdalla, M., Zhou, M., Walker, R., El-Alaoui, M., Angelopoulos, V., ... Schriver, D. (2010, September). Wave and particle characteristics of earthward electron injections associated with dipolarization fronts. *J. Geophys. Res.*, *115*, A09225. doi: 10.1029/2009JA015107
- Denton, R. E., Takahashi, K., Galkin, I. A., Nsumei, P. A., Huang, X., Reinisch, B. W., ... Hughes, W. J. (2006, April). Distribution of density along magnetospheric field lines. *J. Geophys. Res.*, *111*, 4213. doi: 10.1029/2005JA011414
- Douma, E., Rodger, C. J., Blum, L. W., & Clilverd, M. A. (2017, August). Occurrence characteristics of relativistic electron microbursts from SAMPEX observations. *Journal of Geophysical Research (Space Physics)*, *122*(8), 8096-8107. doi: 10.1002/2017JA024067
- Douma, E., Rodger, C. J., Blum, L. W., O'Brien, T. P., Clilverd, M. A., & Blake, J. B. (2019, July). Characteristics of Relativistic Microburst Intensity From SAMPEX Observations. *Journal of Geophysical Research (Space Physics)*, *124*(7), 5627-5640. doi: 10.1029/2019JA026757
- Fu, H. S., Khotyaintsev, Y. V., Vaivads, A., Retinò, A., & André, M. (2013, July). Energetic electron acceleration by unsteady magnetic reconnection. *Nature Physics*, *9*, 426-430. doi: 10.1038/nphys2664
- Fu, X., Cowee, M. M., Friedel, R. H., Funsten, H. O., Gary, S. P., Hospodarsky, G. B., ... Winske, D. (2014, October). Whistler anisotropy instabilities as the source of banded chorus: Van Allen Probes observations and particle-in-cell simulations. *Journal of Geophysical Research (Space Physics)*, *119*, 8288-8298. doi: 10.1002/2014JA020364
- Gabrielse, C., Angelopoulos, V., Runov, A., & Turner, D. L. (2014, April). Statistical characteristics of particle injections throughout the equatorial magnetotail. *J. Geophys. Res.*, *119*, 2512-2535. doi: 10.1002/2013JA019638
- Gan, L., Artemyev, A., Li, W., Zhang, X.-J., Ma, Q., Mourenas, D., ... Wilkins, C. (2023, April). Bursty Energetic Electron Precipitation by High-Order Resonance With Very-Oblique Whistler-Mode Waves. *Geophys. Res. Lett.*, *50*(8), e2022GL101920. doi: 10.1029/2022GL101920
- Gjerloev, J. W. (2012, September). The SuperMAG data processing technique. *Journal of Geophysical Research (Space Physics)*, *117*(A9), A09213. doi: 10.1029/2012JA017683
- Grach, V. S., Artemyev, A. V., Demekhov, A. G., Zhang, X.-J., Bortnik, J., Angelopoulos, V., ... Roberts, O. W. (2022, September). Relativistic Electron Precipitation by EMIC Waves: Importance of Nonlinear Resonant Effects. *Geophys. Res. Lett.*, *49*(17), e99994. doi: 10.1029/2022GL099994
- Grach, V. S., & Demekhov, A. G. (2023, July). Interaction of Relativistic Electrons with Packets of the Electromagnetic Ion Cyclotron Waves of Finite Length and Low Amplitude. *Plasma Physics Reports*, *49*(7), 901-911. doi: 10.1134/S1063780X23600561
- Grigorenko, E. E., Malykhin, A. Y., Shklyar, D. R., Fadanelli, S., Lavraud, B., Panov, E. V., ... Le Contel, O. (2020, September). Investigation of Electron Distribution Functions Associated With Whistler Waves at Dipolarization Fronts in the Earth's Magnetotail: MMS Observations. *Journal of Geophysical Research (Space Physics)*, *125*(9), e28268. doi: 10.1029/2020JA028268
- Hanzelka, M., Li, W., & Ma, Q. (2023, April). Parametric analysis of pitch angle scattering and losses of relativistic electrons by oblique EMIC waves. *Fron-*

- tiers in Astronomy and Space Sciences*, 10, 1163515. doi: 10.3389/fspas.2023.1163515
- Hanzelka, M., & Santolík, O. (2019, June). Effects of Ducting on Whistler Mode Chorus or Exohiss in the Outer Radiation Belt. *Geophys. Res. Lett.*, 46(11), 5735-5745. doi: 10.1029/2019GL083115
- Harid, V., Agapitov, O., Khatun-E-Zannat, R., Gołkowski, M., & Hosseini, P. (2024, March). Complex Whistler-Mode Wave Features Created by a High Density Plasma Duct in the Magnetosphere. *Journal of Geophysical Research (Space Physics)*, 129(3), e2023JA032047. doi: 10.1029/2023JA032047
- Horne, R. B., Thorne, R. M., Glauert, S. A., Albert, J. M., Meredith, N. P., & Anderson, R. R. (2005, March). Timescale for radiation belt electron acceleration by whistler mode chorus waves. *J. Geophys. Res.*, 110, 3225. doi: 10.1029/2004JA010811
- Hosseini, P., Agapitov, O., Harid, V., & Gołkowski, M. (2021, March). Evidence of Small Scale Plasma Irregularity Effects on Whistler Mode Chorus Propagation. *Geophys. Res. Lett.*, 48(5), e92850. doi: 10.1029/2021GL092850
- Hwang, K.-J., Goldstein, M. L., Lee, E., & Pickett, J. S. (2011, April). Cluster observations of multiple dipolarization fronts. *J. Geophys. Res.*, 116, A00I32. doi: 10.1029/2010JA015742
- Johnson, A. T., Shumko, M., Sample, J., Griffith, B., Klumpar, D., Spence, H., & Blake, J. B. (2021, November). The Energy Spectra of Electron Microbursts Between 200 keV and 1 MeV. *Journal of Geophysical Research (Space Physics)*, 126(11), e29709. doi: 10.1029/2021JA029709.1002/essoar.10507432.2
- Kang, N., Artemyev, A. V., Bortnik, J., Zhang, X.-J., & Angelopoulos, V. (2024). The principal role of chorus ducting for night-side relativistic electron precipitation. *ESS Open Archive*. doi: 10.22541/essoar.171691118.84057431/v1
- Ke, Y., Chen, L., Gao, X., Lu, Q., Wang, X., Chen, R., ... Wang, S. (2021, April). Whistler Mode Waves Trapped by Density Irregularities in the Earth's Magnetosphere. *Geophys. Res. Lett.*, 48(7), e92305. doi: 10.1029/2020GL092305
- Kennel, C. F. (1969). Consequences of a magnetospheric plasma. *Reviews of Geophysics and Space Physics*, 7, 379-419. doi: 10.1029/RG007i001p00379
- Le Contel, O., Roux, A., Jacquy, C., Robert, P., Berthomier, M., Chust, T., ... Singer, H. (2009, June). Quasi-parallel whistler mode waves observed by THEMIS during near-earth dipolarizations. *Annales Geophysicae*, 27, 2259-2275. doi: 10.5194/angeo-27-2259-2009
- Le Contel, O., Roux, A., Robert, P., Coillot, C., Bouabdellah, A., de La Porte, B., ... Larson, D. (2008, December). First Results of the THEMIS Search Coil Magnetometers. *Space Sci. Rev.*, 141, 509-534. doi: 10.1007/s11214-008-9371-y
- Li, W., Bortnik, J., Thorne, R. M., & Angelopoulos, V. (2011, December). Global distribution of wave amplitudes and wave normal angles of chorus waves using THEMIS wave observations. *J. Geophys. Res.*, 116, 12205. doi: 10.1029/2011JA017035
- Li, W., & Hudson, M. K. (2019, Nov). Earth's Van Allen Radiation Belts: From Discovery to the Van Allen Probes Era. *Journal of Geophysical Research (Space Physics)*, 124(11), 8319-8351. doi: 10.1029/2018JA025940
- Li, W., Ni, B., Thorne, R. M., Bortnik, J., Green, J. C., Kletzing, C. A., ... Hospodarsky, G. B. (2013, September). Constructing the global distribution of chorus wave intensity using measurements of electrons by the POES satellites and waves by the Van Allen Probes. *Geophys. Res. Lett.*, 40, 4526-4532. doi: 10.1002/grl.50920
- Lorentzen, K. R., Blake, J. B., Inan, U. S., & Bortnik, J. (2001, April). Observations of relativistic electron microbursts in association with VLF chorus. *J. Geophys. Res.*, 106(A4), 6017-6028. doi: 10.1029/2000JA003018

- Lyons, L. R., Nishimura, Y., Zhang, S., Coster, A., Liu, J., Bristow, W. A., ... Hampton, D. L. (2021, October). Direct Connection Between Auroral Oval Streamers/Flow Channels and Equatorward Traveling Ionospheric Disturbances. *Frontiers in Astronomy and Space Sciences*, *8*, 169. doi: 10.3389/fspas.2021.738507
- Lyons, L. R., & Williams, D. J. (1984). *Quantitative aspects of magnetospheric physics*. (Lyons, L. R. & Williams, D. J., Ed.).
- Ma, Q., Li, W., Bortnik, J., Thorne, R. M., Chu, X., Ozeke, L. G., ... Claudepierre, S. G. (2018, March). Quantitative Evaluation of Radial Diffusion and Local Acceleration Processes During GEM Challenge Events. *Journal of Geophysical Research (Space Physics)*, *123*(3), 1938-1952. doi: 10.1002/2017JA025114
- Malaspina, D. M., Ukhorskiy, A., Chu, X., & Wygant, J. (2018, April). A Census of Plasma Waves and Structures Associated With an Injection Front in the Inner Magnetosphere. *J. Geophys. Res.*, *123*, 2566-2587. doi: 10.1002/2017JA025005
- McFadden, J. P., Carlson, C. W., Larson, D., Ludlam, M., Abiad, R., Elliott, B., ... Angelopoulos, V. (2008, December). The THEMIS ESA Plasma Instrument and In-flight Calibration. *Space Sci. Rev.*, *141*, 277-302. doi: 10.1007/s11214-008-9440-2
- Meredith, N. P., Horne, R. B., Sicard-Piet, A., Boscher, D., Yearby, K. H., Li, W., & Thorne, R. M. (2012, October). Global model of lower band and upper band chorus from multiple satellite observations. *J. Geophys. Res.*, *117*, 10225. doi: 10.1029/2012JA017978
- Meredith, N. P., Horne, R. B., Thorne, R. M., & Anderson, R. R. (2003, August). Favored regions for chorus-driven electron acceleration to relativistic energies in the Earth's outer radiation belt. *Geophys. Res. Lett.*, *30*(16), 160000-1. doi: 10.1029/2003GL017698
- Meyer-Reed, C., Blum, L., & Shumko, M. (2023, January). Pitch Angle Isotropy of Relativistic Electron Microbursts as Observed by SAMPEX/HILT: Statistical and Storm-Time Properties. *Journal of Geophysical Research (Space Physics)*, *128*(1), e2022JA030926. doi: 10.1029/2022JA030926
- Millan, R. M., & Thorne, R. M. (2007, March). Review of radiation belt relativistic electron losses. *Journal of Atmospheric and Solar-Terrestrial Physics*, *69*, 362-377. doi: 10.1016/j.jastp.2006.06.019
- Mironova, I. A., Artamonov, A. A., Bazilevskaya, G. A., Rozanov, E. V., Kovaltsov, G. A., Makhmutov, V. S., ... Karagodin, A. V. (2019, January). Ionization of the Polar Atmosphere by Energetic Electron Precipitation Retrieved From Balloon Measurements. *Geophys. Res. Lett.*, *46*(2), 990-996. doi: 10.1029/2018GL079421
- Miyoshi, Y., Hosokawa, S., Kurita, S.-I., Oyama, Y., Ogawa, S., Saito, I., ... Nakamura (2021). Penetration of MeV electrons into the mesosphere accompanying pulsating aurorae. *Scientific Reports*, *11*, 13724. doi: 10.1038/s41598-021-92611-3
- Miyoshi, Y., Saito, S., Kurita, S., Asamura, K., Hosokawa, K., Sakanoi, T., ... Blake, J. B. (2020, November). Relativistic Electron Microbursts as High-Energy Tail of Pulsating Aurora Electrons. *Geophys. Res. Lett.*, *47*(21), e90360. doi: 10.1029/2020GL090360
- Mourenas, D., Artemyev, A. V., Agapitov, O. V., & Krasnoselskikh, V. (2014, April). Consequences of geomagnetic activity on energization and loss of radiation belt electrons by oblique chorus waves. *J. Geophys. Res.*, *119*, 2775-2796. doi: 10.1002/2013JA019674
- Mourenas, D., Artemyev, A. V., Zhang, X. J., Angelopoulos, V., Tsai, E., & Wilkins, C. (2021, November). Electron Lifetimes and Diffusion Rates Inferred From ELFIN Measurements at Low Altitude: First Results. *Journal of Geophysical Research (Space Physics)*, *126*(11), e29757. doi:

10.1029/2021JA029757

- Nakamura, R., Baumjohann, W., Mouikis, C., Kistler, L. M., Runov, A., Volwerk, M., . . . Balogh, A. (2004, May). Spatial scale of high-speed flows in the plasma sheet observed by Cluster. *Geophys. Res. Lett.*, *31*, 9804. doi: 10.1029/2004GL019558
- Ni, B., Li, W., Thorne, R. M., Bortnik, J., Green, J. C., Kletzing, C. A., . . . Soria-Santacruz Pich, M. (2014, July). A novel technique to construct the global distribution of whistler mode chorus wave intensity using low-altitude POES electron data. *J. Geophys. Res.*, *119*, 5685-5699. doi: 10.1002/2014JA019935
- Ni, B., Thorne, R. M., Meredith, N. P., Shprits, Y. Y., & Horne, R. B. (2011, October). Diffuse auroral scattering by whistler mode chorus waves: Dependence on wave normal angle distribution. *J. Geophys. Res.*, *116*, 10207. doi: 10.1029/2011JA016517
- Nishimura, Y., Deng, Y., Lyons, L. R., McGranaghan, R. M., & Zettergren, M. D. (2021, May). Multiscale Dynamics in the High-Latitude Ionosphere. In C. Huang & G. Lu (Eds.), *Ionosphere dynamics and applications* (Vol. 3, p. 49). doi: 10.1002/9781119815617.ch3
- Oyama, S., Kero, A., Rodger, C. J., Clilverd, M. A., Miyoshi, Y., Partamies, N., . . . Saito, S. (2017, June). Energetic electron precipitation and auroral morphology at the substorm recovery phase. *Journal of Geophysical Research (Space Physics)*, *122*(6), 6508-6527. doi: 10.1002/2016JA023484
- Roosnovo, A., Artemyev, A. V., Zhang, X.-J., Angelopoulos, V., Ma, Q., Grimnich, N., . . . Werner, M. (2024, May). Relativistic Electron Precipitation Events Driven by Solar Wind Impact on the Earth's Magnetosphere. *Journal of Geophysical Research (Space Physics)*, *129*(5), e2023JA032257. doi: 10.1029/2023JA032257
- Runov, A., Angelopoulos, V., Gabrielse, C., Zhou, X.-Z., Turner, D., & Plaschke, F. (2013, February). Electron fluxes and pitch-angle distributions at dipolarization fronts: THEMIS multipoint observations. *J. Geophys. Res.*, *118*, 744-755. doi: 10.1002/jgra.50121
- Runov, A., Angelopoulos, V., Sitnov, M. I., Sergeev, V. A., Bonnell, J., McFadden, J. P., . . . Auster, U. (2009, July). THEMIS observations of an earthward-propagating dipolarization front. *Geophys. Res. Lett.*, *36*, L14106. doi: 10.1029/2009GL038980
- Runov, A., Angelopoulos, V., Zhou, X.-Z., Zhang, X.-J., Li, S., Plaschke, F., & Bonnell, J. (2011, May). A THEMIS multicase study of dipolarization fronts in the magnetotail plasma sheet. *J. Geophys. Res.*, *116*, 5216. doi: 10.1029/2010JA016316
- Santolík, O., & Gurnett, D. A. (2003, January). Transverse dimensions of chorus in the source region. *Geophys. Res. Lett.*, *30*(2), 1031. doi: 10.1029/2002GL016178
- Santolík, O., Macúšová, E., Kolmašová, I., Cornilleau-Wehrlin, N., & Conchy, Y. (2014, April). Propagation of lower-band whistler-mode waves in the outer Van Allen belt: Systematic analysis of 11 years of multi-component data from the Cluster spacecraft. *Geophys. Res. Lett.*, *41*, 2729-2737. doi: 10.1002/2014GL059815
- Seppälä, A., Clilverd, M. A., Beharrell, M. J., Rodger, C. J., Verronen, P. T., Andersson, M. E., & Newnham, D. A. (2015, October). Substorm-induced energetic electron precipitation: Impact on atmospheric chemistry. *Geophys. Res. Lett.*, *42*(19), 8172-8176. doi: 10.1002/2015GL065523
- Sergeev, V. A., Kubyshkina, M. V., Semenov, V. S., Artemyev, A., Angelopoulos, V., & Runov, A. (2023, November). Unusual Magnetospheric Dynamics During Intense Substorm Initiated by Strong Magnetospheric Compression. *Journal of Geophysical Research (Space Physics)*, *128*(11), e2023JA031536. doi: 10.1029/2023JA031536

- Sheeley, B. W., Moldwin, M. B., Rassoul, H. K., & Anderson, R. R. (2001, November). An empirical plasmasphere and trough density model: CRRES observations. *J. Geophys. Res.*, *106*, 25631-25642. doi: 10.1029/2000JA000286
- Shen, Y., Artemyev, A. V., Ma, Q., Zhang, X.-J., Mourenas, D., Tsai, E., ... Angelopoulos, V. (2022, November). Inner Belt Wisp Precipitation Measured by ELFİN: Regimes of Energetic Electron Scattering by VLF Transmitter Waves. *Journal of Geophysical Research (Space Physics)*, *127*(11), e2022JA030968. doi: 10.1029/2022JA030968
- Shumko, M., Blum, L. W., & Crew, A. B. (2021, September). Duration of Individual Relativistic Electron Microbursts: A Probe Into Their Scattering Mechanism. *Geophys. Res. Lett.*, *48*(17), e93879. doi: 10.1029/2021GL093879
- Shumko, M., Miyoshi, Y., Blum, L. W., Halford, A. J., Breneman, A. W., Johnson, A. T., ... Spence, H. E. (2023, August). Observation of an Electron Microburst With an Inverse Time-Of-Flight Energy Dispersion. *Geophys. Res. Lett.*, *50*(15), e2023GL104804. doi: 10.1029/2023GL104804
- Stepanov, N. A., Sergeev, V. A., Shukhtina, M. A., Ogawa, Y., Chu, X., & Rogov, D. D. (2021, July). Ionospheric Electron Density and Conductance Changes in the Auroral Zone During Substorms. *Journal of Geophysical Research (Space Physics)*, *126*(7), e29572. doi: 10.1029/2021JA029572
- Streltsov, A. V., & Bengtson, M. T. (2020, October). Observations and Modeling of Whistler Mode Waves in the Magnetospheric Density Ducts. *Journal of Geophysical Research (Space Physics)*, *125*(10), e28398. doi: 10.1029/2020JA028398
- Streltsov, A. V., & Goyal, R. (2021, November). Whistlers in Micro Ducts. *Journal of Geophysical Research (Space Physics)*, *126*(11), e29868. doi: 10.1029/2021JA029868
- Summers, D., Ni, B., & Meredith, N. P. (2007a, April). Timescales for radiation belt electron acceleration and loss due to resonant wave-particle interactions: 1. Theory. *J. Geophys. Res.*, *112*, 4206. doi: 10.1029/2006JA011801
- Summers, D., Ni, B., & Meredith, N. P. (2007b, April). Timescales for radiation belt electron acceleration and loss due to resonant wave-particle interactions: 2. Evaluation for VLF chorus, ELF hiss, and electromagnetic ion cyclotron waves. *J. Geophys. Res.*, *112*, 4207. doi: 10.1029/2006JA011993
- Tao, X., Thorne, R. M., Li, W., Ni, B., Meredith, N. P., & Horne, R. B. (2011, April). Evolution of electron pitch angle distributions following injection from the plasma sheet. *J. Geophys. Res.*, *116*, A04229. doi: 10.1029/2010JA016245
- Tsai, E., Artemyev, A., Angelopoulos, V., & Zhang, X.-J. (2023, August). Investigating Whistler-Mode Wave Intensity Along Field Lines Using Electron Precipitation Measurements. *Journal of Geophysical Research (Space Physics)*, *128*(8), e2023JA031578. doi: 10.1029/2023JA031578
- Tsai, E., Artemyev, A., Ma, Q., Mourenas, D., Agapitov, O., Zhang, X.-J., & Angelopoulos, V. (2024, March). Key Factors Determining Nightside Energetic Electron Losses Driven by Whistler-Mode Waves. *Journal of Geophysical Research (Space Physics)*, *129*(3), e2023JA032351. doi: 10.1029/2023JA032351
- Tsai, E., Artemyev, A., Zhang, X.-J., & Angelopoulos, V. (2022, May). Relativistic Electron Precipitation Driven by Nonlinear Resonance With Whistler-Mode Waves. *Journal of Geophysical Research (Space Physics)*, *127*(5), e30338. doi: 10.1029/2022JA030338
- Tsai, E., & et al. (2024). Remote Sensing of Electron Precipitation Mechanisms Enabled by ELFİN Mission Operations and ADCS Design. *Engineering Archive*. doi: 10.31224/3487
- Ukhorskiy, A. Y., Sorathia, K. A., Merkin, V. G., Crabtree, C., Fletcher, A. C., Malaspina, D. M., & Schwartz, S. J. (2022, March). Cross-scale energy cascade powered by magnetospheric convection. *Scientific Reports*, *12*, 4446. doi:

10.1038/s41598-022-08038-x

- Verronen, P. T., Kero, A., Partamies, N., Szelag, M. E., Oyama, S.-I., Miyoshi, Y., & Turunen, E. (2021, October). Simulated seasonal impact on middle atmospheric ozone from high-energy electron precipitation related to pulsating aurorae. *Annales Geophysicae*, *39*(5), 883-897. doi: 10.5194/angeo-39-883-2021
- Wilkins, C., Angelopoulos, V., Runov, A., Artemyev, A., Zhang, X. J., Liu, J., & Tsai, E. (2023, October). Statistical Characteristics of the Electron Isotropy Boundary. *Journal of Geophysical Research (Space Physics)*, *128*(10), e2023JA031774. doi: 10.1029/2023JA031774
- Yu, Y., Cao, J., Pu, Z., Jordanova, V. K., & Ridley, A. (2022, December). Mesoscale Electrodynamic Coupling of the Earth Magnetosphere-Ionosphere System. *Space Sci. Rev.*, *218*(8), 74. doi: 10.1007/s11214-022-00940-0
- Yu, Y., Jordanova, V. K., McGranaghan, R. M., & Solomon, S. C. (2018, July). Self-Consistent Modeling of Electron Precipitation and Responses in the Ionosphere: Application to Low-Altitude Energization During Substorms. *Geophys. Res. Lett.*, *45*(13), 6371-6381. doi: 10.1029/2018GL078828
- Zhang, X., Angelopoulos, V., Artemyev, A. V., & Liu, J. (2018, September). Whistler and Electron Firehose Instability Control of Electron Distributions in and Around Dipolarizing Flux Bundles. *Geophys. Res. Lett.*, *45*, 9380-9389. doi: 10.1029/2018GL079613
- Zhang, X., Angelopoulos, V., Artemyev, A. V., & Liu, J. (2019, November). Energy Transport by Whistler Waves Around Dipolarizing Flux Bundles. *Geophys. Res. Lett.*, *46*(21), 11,718-11,727. doi: 10.1029/2019GL084226
- Zhang, X.-J., Angelopoulos, V., Artemyev, A., Mourenas, D., Agapitov, O., Tsai, E., & Wilkins, C. (2023, January). Temporal Scales of Electron Precipitation Driven by Whistler-Mode Waves. *Journal of Geophysical Research (Space Physics)*, *128*(1), e2022JA031087. doi: 10.1029/2022JA031087
- Zhang, X.-J., Angelopoulos, V., Mourenas, D., Artemyev, A., Tsai, E., & Wilkins, C. (2022, May). Characteristics of Electron Microburst Precipitation Based on High-Resolution ELFIN Measurements. *Journal of Geophysical Research (Space Physics)*, *127*(5), e30509. doi: 10.1029/2022JA030509
- Zhang, X.-J., Artemyev, A., Angelopoulos, V., Tsai, E., Wilkins, C., Kasahara, S., ... Matsuoka, A. (2022, March). Superfast precipitation of energetic electrons in the radiation belts of the Earth. *Nature Communications*, *13*, 1611. doi: 10.1038/s41467-022-29291-8
- Zou, Y., Zhang, X.-J., Artemyev, A. V., Shen, Y., & Angelopoulos, V. (2024, July). The Key Role of Magnetic Curvature Scattering in Energetic Electron Precipitation During Substorms. *Geophys. Res. Lett.*, *51*(14), e2024GL109227. doi: 10.1029/2024GL109227